Gene Expression, Vol. 14, pp. 345–359
Printed in the USA.

1052-2166/10 $90.00 + .00
DOI: 10.3727/105221610X12718619643013
E-ISSN 1555-3884
www.cognizantcommunication.com

Transcritpional Effects of S100B on Neuroblastoma Cells: Perturbation of Cholesterol Homeostasis and Interference on the Cell Cycle

C. BERNARDINI,*[1] W. LATTANZI,*[1] R. BUSINARO,† S. LEONE,‡ V. CORVINO,* G. SORCI,§ G. LAURO,‡ L. FUMAGALLI,† R. DONATO,§ AND F. MICHETTI*

**Institute of Anatomy and Cell Biology, Catholic University, Rome, Italy*
†Department of Cardiovascular Sciences, University La Sapienza, Rome, Italy
‡Department of Biology, University Roma TRE, Rome, Italy
§Department of Experimental Medicine and Biochemical Sciences, Sect. Anatomy, University of Perugia, Perugia, Italy

S100B is a Ca^{2+} binding protein mainly secreted by astrocytes in the vertebrate brain that is considered a multifunctional cytokine and/or a damage-associated molecular pattern (DAMP) protein and a marker of brain injury and neurodegeneration when measured in different body fluids. It has been widely shown that this protein can exert diverse effects in neural cultures depending on its concentration, having detrimental effects at micromolar concentrations. The molecular mechanisms underlying this effect are still largely unknown. This study attempts to delineate the genome-wide gene expression analysis of the events associated with exposure to micromolar concentration of S100B in a human neuroblastoma cell line. In this experimental condition cells undergo a severe perturbation of lipid homeostasis along with cell cycle arrest. These mechanisms might reasonably mediate some aspects of the S100B-related detrimental effects of S100B, although obvious differences between mature neurons and neuroblastoma cells have to be considered.

Key words: Microarray; Cholesterol biosynthesis; Lipid homeostasis; Cell cycle

INTRODUCTION

S100B is a Ca^{2+} binding protein of the EF-hand type concentrated in glial cells in the nervous system, being also produced by definite extraneural cell types (34). S100B is mainly produced and secreted by astrocytes in the vertebrate brain where it exerts paracrine effects on neurons along with possible autocrine effects (22), being considered a multifunctional cytokine and/or a damage-associated molecular pattern (DAMP) protein. In particular, studies in neural cultures revealed a detrimental effect of extracellular S100B at micromolar concentration, and conversely, a trophic effect at pico- and nanomolar concentrations was observed (15,42,46).

S100B gene maps on the long arm of chromosome 21 (21q22.3); thus, an increase in gene expression for the protein has been related to the processes associated with Down syndrome (DS) (1), the protein being also overexpressed in the amniotic fluid of fetuses with trisomy 21 (20). A possible role of S100B has also been proposed in Alzheimer's disease (AD), which is known to share some pathogenic aspects with DS. It is noteworthy in this respect that brains from AD patients con-

[1]These authors contributed equally to this work.

Address correspondence to Prof. Fabrizio Michetti, M.D., Institute of Anatomy and Cell Biology, Catholic University, L.go F. Vito, 1, 00168 Rome, Italy. Tel: +39 06 30155848; Fax: +39 06 30154813; E-mail: fabrizio.michetti@rm.unicatt.it

tain elevated levels of S100B mRNA and protein and that β-amyloid (Aβ) has been shown to stimulate the synthesis of S100B (15,36,42,46). In addition, transgenic mice overexpressing S100B have been shown to exhibit an increased susceptibility to Aβ (13) and to perinatal hypoxia-ischemia (47).

Increased levels of S100B in biological fluids have been demonstrated to constitute a reliable index of active brain injury (33), although the role of this protein in neuropathological processes is still unclear. Several brain disorders, including trauma, ischemia, neurodegenerative diseases, psychiatric disorders, and perinatal brain damage, have been described as being associated with peripheral increases in S100B. Furthermore, S100B levels generally correlate with the severity of brain injury and have been reported to have a predictive association with adverse neurological outcomes (32,42). Despite compelling evidences suggesting that S100B overexpression and increased release lead to neuronal injury, poor information is currently available on the molecular events evoked by extracellular S100B in target cells.

Microarray analysis can be considered a powerful investigative tool as it covers the simultaneous expression profiling of the entire genome and appears to be especially useful for a comprehensive investigation of the intracellular function of bioactive molecules. The aim of this study is therefore to clarify the general molecular mechanisms elicited by S100B in neural cells at a concentration regarded as being toxic, by means of a genome-wide expression analysis performed using microarray technology. For this purpose, we treated LAN-5 human neuroblastoma cells, which have already been shown to be responsive to the recombinant S100B protein (9). Data will be shown indicating essentially an S100B-dependent perturbation of cholesterol homeostasis accompanied by interference in the cell cycle. This gene modulation could underlie the detrimental effects of the protein in this model.

MATERIALS AND METHODS

Peptide Synthesis

Recombinant S100B was expressed in *Escherichia coli* BL21 using the S100B expression vector sequence (50) and purified as described elsewhere (14,26). The recombinant peptide was passed through END-X B15 Endotoxin Affinity Resin column (Associated of Cape Cod) to remove contaminating bacterial endotoxin. Residual bacterial endotoxin was evaluated using the chromogenic Limulus amoebocyte lysates assay (Associated of Cape Cod), resulting in bacterial endotoxin concentration <0.2 pg/mg.

Cell Cultures and Treatments

The LAN-5 neuroblastoma cell line was grown in Dulbecco's modified Eagle medium (DMEM) supplemented with 2 mM glutamine, 40 μg/ml gentamicin, and 10% heat-inactivated fetal calf serum (FCS) (all chemicals were purchased from Sigma, St. Louis, MO) in an atmosphere of 5% CO_2 at 37°C.

Cells were plated at a $10^4/cm^2$ seeding density and incubated at 37°C for 24 h in a humidified incubator with 5% CO_2. S100B protein treatments were carried out using scalar concentrations ranging from 0.5 nM to 5 μM for cell viability assay (see following paragraph). Cells were treated with 5 μM S100B and harvested 48 h after the treatment for RNA isolation. Untreated cells were cultured as controls.

Cell Viability Assay

Cell survival was determined by the MTT (3-[4,5-dimethylthiazol-2-yl]-2,5-diphenyl tetrazolium bromide) reduction assay (24). For this purpose cells were plated in 24-well plates and treated with scalar concentrations (0.5 nM to 5 μM) of S100B. After 48 h cells were incubated with 100 μl RPMI containing 0.5 mg/ml of MTT for 3 h at 37°C in a humidified incubator containing 5% CO_2. The reaction was stopped by adding 100 μl of lysis buffer [20% (w/v) SDS in 50% of *N*,*N*-dimethylformamide, pH to 4.79] to each well. The amount of MTT formazan product was determined by measuring absorbance at 570 nm using a microplate reader (Bio-Rad, Hercules, CA). The viability was determined as the percentage of absorbance measured in treated cultures compared with that of untreated controls.

Microarray Analysis

Total RNA, isolated from control and treated cells (5 μM S100B), in triplicate experiments (six samples), was analyzed by Affymetrix Genechip microarray, as previously described (29). Briefly, total RNA was isolated using RNeasy Mini Kit (Qiagen Inc., Valencia, CA) according to the manufacturer's instructions. In order to avoid genomic DNA in samples, RNA was digested with amplification grade DNase I (Qiagen). The yield of RNA isolation was determined using spectrophotometry (Beckman DU800, Beckman Coulter, Inc., Fullerton, CA). The quality and integrity of total RNA were assessed using the Agilent 2100 Bioanalyzer (Agilent Technologies, Palo Alto, CA). The syntheses of cDNA and biotinylated cRNA were performed according to the protocols provided by the manufacturer (Affymetrix, Santa Clara, CA). Also cRNA quality control was performed using the Bioanalyzer (Agilent Technologies). Bio-

tinylated fragmented cRNA probes were hybridized to the Human Genome Focus Array (Affymetrix), which contained probe sets for over 8,700 known transcripts and expressed sequence tags. Hybridization was performed at 45°C for 16 h in a hybridization oven (Affymetrix). The Genechips were then automatically washed and stained with streptavidin–phycoerythrin conjugate in an Affymetrix Genechip Fluidics Station. Fluorescence intensities were scanned with a Affymetrix GeneChip Scanner 3000. Hybridizations were carried out independently for each condition using three biological replicates, according to MIAME guidelines (8).

Data Analysis Preprocessing

Gene expression Affymetrix data were then analyzed using Partek Genomics Suite software (version 6.4 © 2009 Partek Inc., St. Louis, MO). For this purpose CEL files were imported using the default Partek normalization parameters. Probe-level data were preprocessed, including background correction, normalization, and summarization (51), using robust multiarray average (RMA) analysis; subsequent data normalization was performed across all arrays using quantile normalization (7,28). The normalized probe intensity values were then compiled, or summarized, within each probe set, using the median polish technique, to generate a single measure of expression (28). These expression measures were then log transformed, base 2.

Data Analysis Differential Expression Analysis

Quality control on data set was performed using Principal Component Analysis (PCA) on all the genes in order to test the segregation efficiency. The list resulting from the statistical analysis of microarray data (see following section) was annotated according to functional roles or biological processes according to the Gene Ontology Consortium directions (4).

In addition, the gene list was analyzed by Ingenuity Pathway Analysis (IPA), Ingenuity® Systems (www.ingenuity.com). This generated functional networks and canonical pathways that connect the differentially expressed genes, using the IPA Knowledge base, in which the interactions are supported by peer-reviewed publications and which contains over 1.4 million interactions between genes, proteins, and drugs. Scores were assigned allowing ranking of the networks, using a Fisher's right tailed exact test. First, data were subdued to IPA Functional Analysis, enabling to associate biological functions and diseases to the experimental results. The canonical pathways output allowed to display the most significant canonical pathways across the entire dataset, assigning a *p*-value indicating the statistical significance of the association. Moreover, the software allowed for toxicity analysis; that is, it helped to explain and delineate the cell response, mechanism of action, and mechanism of toxicity of a molecule (S100B) in a biological system (LAN-5 cells). In fact, this output listed all molecules in the data set that are known to be involved in a particular type of toxicity, based on IPA database.

Real-Time PCR

Two-step real-time PCR was carried out in order to validate gene expression results obtained by microarray analysis, using three independent replicate RNA samples generated from LAN-5 cells treated with 5 μM S100B at the same time point (48 h). In addition, in order to evaluate the transcriptional modulation induced by subtoxic concentrations of S100B, the expression of selected genes was assessed by means of real-time PCR in LAN-5. For this purpose cells were cultured in presence of 50 nM S100B and gene expression was measured after 48 h. Untreated cells served as controls. All experiments were performed in triplicate.

Real-time PCR was also used to assess the activation of the S100B Receptor for Advanced Glycosylation End-products (RAGE) in the same experiments.

For these purposes, single-strand cDNA was synthesized from 1 μg total RNA using SuperScript™ III First-Strand Synthesis System (Invitrogen, Carlsbad, CA,) using random hexamers, following the manufacturer's instructions. In order to rule out genomic DNA contamination, no-reverse controls (i.e., RT reactions carried out in the absence of the reverse transcriptase enzyme) were added for each sample. Thereafter, 1 μl of a 1:10 dilution of the single-stranded cDNA (corresponding to 20 ng of total RNA) was used for real-time PCR, performed in a reaction volume of 20 μl using the SYBR green PCR master mix (Applied Biosystem, Foster City, CA) and 1 μM of both forward and reverse primers. The analysis was performed on an ABI Prism 7900 Sequence Detection System (Applied Biosystem).

The following genes were selected for validation, as either being indicative of the main functional groups of modulated transcripts or exerting the highest levels of modulation: ATP-binding cassette subfamily G member 1 (ABCG1), cyclin A2 (CCNA2), retinoblastoma like-2 (RBL2); mevalonate(diphospho)decarboxylase (MVD; EC4.1.1.4), 3-hydroxy-3-methylglutaryl-coenzyme A synthase 1 (HMGCS1; EC2.3.3.10), 3-hydroxy-3-methylglutaryl-coenzyme A reductase (HMGCR; EC2.7.11.31), 7-dehydro-

cholesterol reductase (DHCR7; EC1.3.1.21), 24-dehydrocholesterol reductase (DHCR24; EC1.3.1.71), farnesyl-diphosphate farnesyltransferase 1 (FDFT1; EC2.5.1.21), squalene epoxidase (SQLE; EC1.14.99.7). The glyceraldehyde-3-phosphate dehydrogenase (GAPDH; EC 1.2.1.59) gene was used as an endogenous control to correct for potential variation in RNA loading or efficiency of the amplification, as it showed the steadiest expression in all conditions across all the standard housekeeping genes present in the microarray data.

The tested genes and sequences of the corresponding primer sets were as follows: ABCG1_F, 5′-tgaggatttgggtctgaac-3′ and ABCG1_R, 5′-ctgctgggttgtggtaggtt-3′; CCNA2_F, 5′-ttattgctggagctgccttt-3′ and CCNA2_R, 5′-tattcaggccagctttgtcc-3′; RBL2_F, 5′-tcttcctttaggagggagttatc-3′ and RBL2_R, 5′-gccaggaacacccaaaaata-3′; MVD_F, 5′-tgcaccaggaccagttaaaa-3′ and MVD_R, 5′-tgaagtccttgctgatgacg-3′; HMGCS1_F, 5′-gggccaaatgctcctttaat-3′ and HMGCS1_R, 5′-gttgcatatgtgtcccacga-3′; HMGCR_F, 5′-gacctttccagagcaagcac-3′ and HMGCR_R, 5′-gagttggaactgagggcaaa-3′; DHCR7_F, 5′-cgtctctccctgacttctgc-3′ and DHCR7_R, 5′-ctcctacgtagccgggtaga-3′; DHCR24_F, 5′-gatgggtgtggcagtgtatg-3′ and DHCR24_R, 5′-cccatgaccaaagaagaaa-3′; FDFT1_F, 5′-catggagagcaaggagaagg-3′ and FDFT1_R, 5′-ggagatcgttgggaagtcct-3′; SQLE_F, 5′-ccatcacggaagattcatca-3′ and SQLE_R, 5′-ctctgccatagctgctttcc-3′; RAGE_F, 5′-gtgctgatcctccctgagatag-3′; RAGE_R, 5′-acagctgtaggttccctggtc-3′ GAPDH_F, 5′-tggaaggactcatgaccaca-3′ and GAPDH_R, 5′-gtcttctgggtggcagtgat-3′.

The PCR conditions were as follows: an initial incubation at 50°C for 2 min and 95°C for 10 min followed by 40 cycles at 94°C for 15 s and 60°C for 1 min. All reactions were performed in triplicate. Standard curves were generated for all the assays to verify PCR efficiency.

The threshold cycle, CT, which correlates inversely with the levels of target mRNA, was measured as the cycle number at which the reporter fluorescence emission exceeded a preset threshold level. The amplified transcripts were quantified using the comparative CT method as previously described, with the formula for relative fold change = $2^{-\Delta\Delta CT}$, where ΔCT = [ΔCT gene of interest (treated sample) – ΔCT GAPDH RNA (treated sample)] – [ΔCT gene of interest (control sample) – ΔCT GAPDH (control sample)]. ΔCT represents the mean CT value of each sample (30).

Statistical Analysis

In the cell viability assay, statistical significance of count variations between controls and treated groups was calculated using one-way ANOVA followed by post hoc comparisons by means of Tukey-HSD test, with a significance level of $p < 0.05$. Statistical analysis of microarray data was performed using algorithms implemented in the Partek Genomic Suite software. Differential expression levels were detected using a one-way ANOVA. A restricted gene list was then generated from the intersection of two criteria: *p*-value cutoff <0.05 and mean change in signal intensity of 1.1-fold or greater, between the treatment and the control group.

RESULTS

Effects of S100B Treatment on Cell Survival

The number of viable cells was assessed by means of MTT colorimetric assay 48 h after S100B treatment. Results, based on mean values plus standard deviation of OD measurements obtained from quadruplicate experiments for each S100B concentration, are shown in Figure 1. Slight changes in cell viability could be measured in cells treated with nanomolar concentrations of S100B, while a significantly reduced number of viable cells was detected at the higher concentrations of S100B (>1 μM, see Fig. 1). These results indicated that micromolar concentrations of S100B are able to significantly affect the viability of neuroblastoma cells, in accordance with well-established data in the literature. The highest tested concentration (5 μM) of the protein was therefore used for the microarray analysis experiments.

Genome-Wide Transcriptional Effects of S100B

In order to test the effects of S100B exposure on gene expression, microarray analysis was performed on RNA isolated from LAN-5 cells treated with S100B, using an active concentration of 5 μM, for 48 h. Three technical replicates per each experimental condition (cells treated with the protein and negative controls) were run, so that a total number of six arrays were analyzed.

The complete raw data set obtained by microarray analysis was submitted to the "Gene Expression Omnibus" (GEO) database (http://www.ncbi.nlm.nih.gov/geo/, accession number GSE15218).

The data set was analyzed by unsupervised PCA in order to check the sample's segregation, which proved to be efficient (data not shown).

We then analyzed genes modulated in treated cells using one-way ANOVA as described in Materials and Methods. The overall number of modulated genes resulting in the dataset was 401, with 85 transcripts being upregulated and 316 downregulated. All

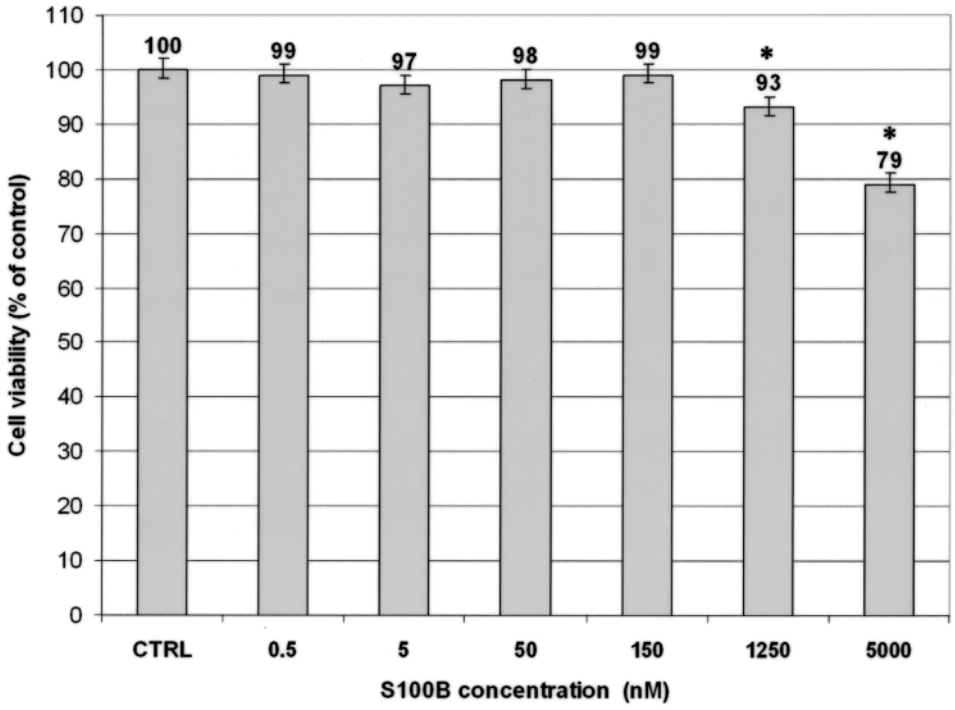

Figure 1. MTT cell viability assay. MTT cell viability assay on LAN-5 treated with scalar concentrations of S100B. Data are mean ± SD from three separate experiments performed in quadruplicate. *Groups that differ significantly from control group, $p < 0.05$.

genes in this dataset were annotated based on their biological function, allowing the categorization of 12 distinct groups (Fig. 2). In particular, the gene expression profiling suggests that S100B in this experimental model seems to modulate several biological activities related to lipid homeostasis and cell cycle.

Functional Analysis

Lipid Metabolism and Homeostasis. The annotated gene list included 40 genes related to cholesterol, fatty acid and steroid biosynthesis, 35 of them being downregulated and 5 upregulated (EHHADH, ABCG1, STXBP3/MUNC18C, ABCA4, PLCL1) (Table 1).

In particular 15 downregulated genes (CYP51A1, DHCR7, DHCR24, FDFT1, FDPS, HMGCR, HMGCS1, IDI1, LSS, MVD, NSDHL, SC4MOL, SC5DL, SQLE, HSD17B7) code for enzymes involved in cholesterol metabolism (Fig. 3). In particular, HMGCR codes for the key enzyme that catalyzes the rate-limiting step of the biosynthetic pathway. It is also interesting that the expression of DHCR24, also known as selective Alzheimer disease indicator-1 (Seladin-1), has been associated with AD-related neurodegeneration (23). This gene codes for the 3β-hydroxysterol-Δ24 reductase, which catalyzes the reduction of desmosterol to produce cholesterol. In addition, five downregulated genes are related to cerebral and peripheral cholesterol and lipoprotein transport and homeostasis (LDLR, ABCG4, APOE, APOA4, BACE1), which are also implicated in the amyloid precursor protein (APP) signaling. The choline kinase alpha (CHKA) gene, coding for the enzyme that catalyzes the first steps of phosphatidylcholine and sphyngomyelin synthesis, was also downregulated in this group. Finally, the gene coding for the lipid myeloperoxidase (MPO) was downregulated; this enzyme is thought to be involved in the early steps of the inflammatory process leading to amyloidogenesis (12).

Cell Cycle Regulation. The annotated gene list comprised 32 genes related to cell cycle regulation, apoptosis, and cell death. In particular, five of them (CDKN2A, RB1, RAD17, RBL2, MOAP1) were upregulated and 27 downregulated (Table 2).

The list of genes that were positively regulated in the dataset included retinoblastoma 1 (RB1) and retinoblastoma-like 2 (RBL2, p130), which are a negative regulator of the cell cycle; cyclin-dependent signaling kinase inhibitor 2A (CDKN2A, p16), an inhibitor of CDK4 kinase; RAD17 homolog (*S. pombe*) (RAD17), a member of a family of essential factors that activate cell cycle checkpoint. Finally, this group also contained the modulator of apoptosis

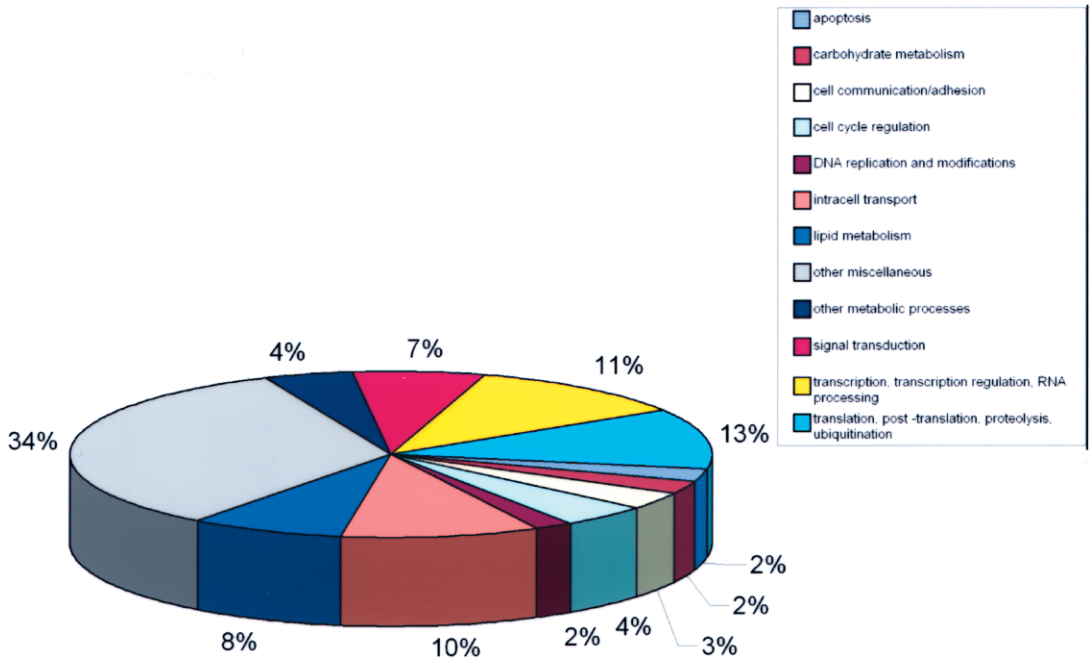

Figure 2. GEO Biological Processes pie chart. All genes resulting from microarray analysis included in the selected list are categorized based on Gene Ontology Biological processes annotations.

1 gene (MOAP1), involved in caspase-dependent apoptosis.

An overall number of 27 transcripts coding for proteins involved in cell cycle regulation were downregulated. In particular, six genes are annotated as regulators of G_1/S transition of mitotic cell cycle (INHBA, RCC1, DBF4, GSPT1, TNXA, TNXB); two genes belong to the cyclin family (CCNA2, CCNB2) and two are annotated in apoptotic pathways (MYC, GAS2). Moreover, the polo-like kinase 1 (PLK1) gene is involved in G_2/M arrest. Finally, the CDC28 protein kinase regulatory subunit 2 (CKS2) is an essential component of cyclin/cyclin-dependent kinase complexes and contributes to cell cycle control.

IPA Analysis

The restricted list comprising 401 genes from the previous analytical steps was then analyzed using Ingenuity System software, with default statistical significance setting ($p < 0.05$). The IPA-based Functional Analysis provided an overview of the functions that are more significantly involved in the experimental model. Based on this analysis, the more relevant molecular functions were found in the cell cycle category, which includes a distinct subcategory corresponding to different phases, with a p-value ranging from 4.98×10^{-2} to 1.51×10^{-4}. IPA also identified a number of canonical signaling pathways that were most significantly affected (Fig. 4, top). The highest score in this analysis was obtained for steroid biosynthesis ($p = 7.16 \times 10^{-7}$) and liver X receptor/retinoid X receptor (LXR/RXR) activation (6.67×10^{-3}). The LXRs α and β are oxysterol-activated nuclear receptors that play an important role in the control of cellular and whole-body cholesterol homeostasis. In addition, IPA allowed the delineation of putative toxicity mechanisms induced by S100B treatment in this cellular model. Also in this list, cholesterol biosynthesis and LXR/RXR activation achieved the highest scores (Fig. 4, bottom).

Real-Time Gene Expression Validation

Gene expression results obtained by microarray analysis were also validated by real-time PCR performed on 10 selected transcripts. The assay confirmed the modulated expression of the target genes tested, showing consistent alignment with the trends shown in the microarray analysis (Fig. 5). Moreover, the expression of selected genes, which resulted downregulated at micromolar concentration of S100B, was also analyzed in LAN-5 cells treated with 50 nM S100B for 48 h. The result showed that six genes (HMGCR, HMGCS1, MVD, FDFT1, SQLE, DHCR7) were upregulated, showing an opposite trend of gene expression than was observed in the 5 μM (Fig. 6). The remaining four genes (DHCR24, RBL2, CCNA2, ABCG1) were not significantly modulated in cells exposed to nanomolar concentrations of S100B.

Finally, considering the higher sensitivity of the technique, we used real-time PCR to quantify the expression of the RAGE gene, as microarray data did not suggest a significant modulation of the S100B receptor gene. The RAGE gene was found to be slightly upregulated in cells treated with either 5 μM or 50 nM of the recombinant peptide compared with controls, with a fold change variation of 1.80 and 2.20, respectively.

DISCUSSION

S100B has been reported to play multiple functions in the nervous system, being secreted by astrocytes and acting as a cytokine and/or a DAMP protein. Although many hypotheses have been formulated, several aspects regarding the functions of S100B are still controversial. In particular, the molecular mediators of its intracellular action are still largely unknown (15,46).

The results obtained in this study provide the first description of the genome-wide transcriptional modulation induced by high concentrations (the "Hyde face") of S100B in LAN-5 neuroblastoma cells. In different cellular models it has been demonstrated that S100B protein can influence the expression of selected genes either via the activation of RAGE (45) or via a RAGE-independent manner (44).

In this experimental model, the most significant gene modulation induced by micromolar S100B lev-

TABLE 1
GENES INVOLVED IN LIPID METABOLISM AND HOMEOSTASIS

Gene Symbol	GenBank	Fold Change	*p*-Value	Gene Ontology Biological Process
CHKA	NM_001277	−1.16	0.0024	lipid metabolic process
HMGCS1	NM_001098272	−2.16	0.0012	lipid metabolic process
SC4MOL	NM_001017369	−1.93	0.0007	fatty acid metabolic process
FDFT1	NM_004462	−1.80	0.0001	steroid biosynthetic process
HMGCR	NM_000859	−1.60	0.0003	steroid biosynthetic process
DHCR7	NM_001360	−1.59	0.0048	blood vessel development
DHCR24	NM_014762	−1.41	0.0029	steroid biosynthetic process
SQLE	NM_003129	−1.55	0.0073	metabolic process
IDI1	NM_004509	−1.48	0.0030	steroid biosynthetic process
CYP51A1	NM_00786	−1.45	0.0056	steroid biosynthetic process
FDPS	NM_002004	−1.44	0.0036	steriod biosynthetic process
LSS	NM_001001438	−1.44	0.0105	steriod biosynthetic process
SC5DL	NM_001024956	−1.43	0.0018	lipid metabolic process
MVD	NM_002461	−1.34	0.0045	steroid biosynthetic process
NSDHL	NM_001129765	−1.25	0.0225	hair follicle development
MPO	NM_000250	−1.12	0.0132	antiapoptosis
EHHADH	NM_001966	1.11	0.0195	lipid metabolic process
ABCG4	NM_004827	−1.19	0.0350	transport
ABCG1	NM_004915	2.08	0.0002	transport/lipid
BACE1	NM_012104	−1.13	0.0058	proteolysis
CHRND	NM_000751	−1.15	0.0172	transport
GABRE	NM_004961	−1.13	0.0387	transport
LDLR	NM_000527	−1.25	0.0117	protein amino acid O-linked glycosylation
APOA4	NM_000482	−1.15	0.0408	innate immune response in mucosa
APOE	NM_00041	−1.11	0.0270	response to reactive oxygen species
HSD17812	NM_016142	−1.13	0.0127	steroid biosynthetic process
HSD1787	NM_016371	−1.58	0.0006	steroid biosynthetic process
STXBP3	NM_007269	1.24	0.0209	transport
INSIG1	NM_005542	−1.57	0.0031	lipid metabolic process
DHCR24	NM_014762	−1.14	0.0029	steroid biosynthetic process
C14orf1	NM_007176	−1.33	0.0028	steroid biosynthetic process
FADS2	NM_004265	−1.30	0.0305	lipid metabolic process
BDH2	NM_020139	−1.17	0.0007	fatty acid β-oxidation
TM7SF2	NM_003273	−1.16	0.0425	steroid biosynthetic process
CEL	NM_001807	−1.15	0.0051	lipid metabolic process
ACOT7	NM_007274	−1.11	0.0291	lipid metabolic process
ELOVL5	NM_021814	−1.10	0.0140	fatty acid biosynthetic process
AGPAT2	NM_001012727	−1.10	0.0009	phospholipid metabolic process
ABCA4	NM_000350	1.11	0.0344	phospholipid transfer to membrane
PLCL1	NM_001114661	1.12	0.0196	lipid metabolic process

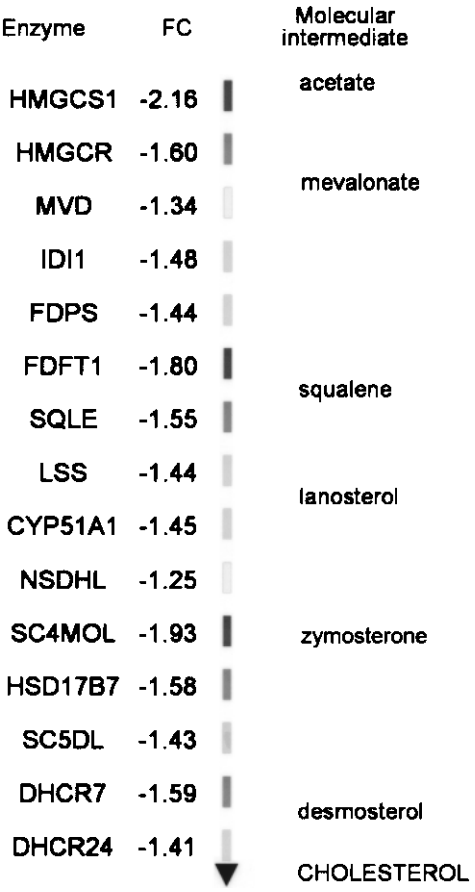

Figure 3. Cholesterol biosynthetic pathway. Genes coding for cholesterologenic enzymes downregulated in this model are listed on the left side of the figure with the corresponding fold change (FC); the most relevant molecular intermediates of the metabolic pathway are listed on the right.

els occurred for genes involved in lipid homeostasis, including LXR signaling, LDL and apolipoprotein trafficking, and cholesterol metabolism and transport. The influence exerted on these genes might reasonably mediate the detrimental effects exerted by micromolar S100B on LAN-5 cells. In particular, our results indicate the inhibition of intracellular cholesterol production and extracellular cholesterol uptake. The transcriptional modulation of cholesterol efflux from cells would result unclear, as ABCG1 and ABCG4 showed opposite trends of expression. Nonetheless, based on the entity of expression variation (FC) and on statistical significance of data (p-value), ABCG1 upregulation was among the most noteworthy data emerging from the gene list (Table 1). Taken together, these data supported the idea of a reduction of intracellular cholesterol in this model. It has been widely demonstrated that a certain level of cholesterol inside the cell is essential for plasma membrane integrity, as reduced cholesterol increases membrane fluidity and cell vulnerability to stress and toxic noxae (3). In this respect, one of the most studied pathological situations is the involvement of the amyloidogenic pathway leading to neural toxicity in AD pathogenesis (10). High cholesterol levels in the extracellular compartment are currently regarded to represents a risk factor for AD (40). On the other hand, it has been demonstrated that cholesterol in the plasma membrane confers protection against Aβ toxicity, increasing membrane stiffness and counteracting the channel-forming activity of the toxic Aβ peptides, thus reducing Ca^{2+} influx (3,37,38). These results could also support previous data showing that micromolar concentrations of S100B increase susceptibility of LAN-5 cells exposed to extracellular Aβ (9).

Within the cholesterologenic enzymes, the Seladin-1 gene was significantly downregulated (FC 1.41; $p = 0.0029$) in our experimental model. This gene, involved in the final steps of cholesterol biosynthesis, was originally identified and named after its selective downregulation in brain areas implicated in the AD neurodegenerative process (23). In addition, its overexpression in culture has been shown to be protective against Aβ toxicity, inducing membrane cholesterol enrichment in the plasma membrane of neural cells (11,23). Seladin-1 has also been demonstrated to be important in the formation of cholesterol-enriched lipid rafts, required for several signaling pathways, being also an LXR target gene (48). The endogenous LXR signaling pathway, which is among the most significantly downregulated canonical pathways in our model, is believed to impact the pathogenesis of neurodegenerative disorders. In particular, LXRs are known to modulate APP processing and decrease Aβ accumulation, although comprehensive reports on LXR functions in the brain are still lacking (49,52). In this model the downregulation of Seladin-1 gene could be reasonably connected to the downregulation of the LXR signaling pathway (48), although further studies aimed at investigating all the transcription factors acting specifically on the DHCR24 promoter could better address this issue. Moreover, other authors showed that the expression of DHCR24 gene is reduced in selected brain regions degenerated in AD patients and is associated with tau protein hyperphosphorylation (27).

It has been recently demonstrated that micromolar S100B concentrations induces tau protein hyperphosphorylation through the RAGE-dependent disruption of Wnt signaling in human neural stem cells, suggesting a new possible direct connection between the S100B protein and formation of neurofibrillary tangles in the pathogenesis of AD (17). It should also be noted that in vitro and in vivo studies suggest that intracellular cholesterol homeostasis has an effect on

TABLE 2
GENES INVOLVED IN CELL CYCLE REGULATION

Gene Symbol	GenBank	Fold Change	*p*-Value	Gene Ontology Biological Process	Pathway
CHKA	NM_001277	−1.16	0.0024	lipid metabolic process	acetylcholine synthesis
CASP1	NM_001223	−1.11	0.0373	proteolysis	apoptosis
MYC	NM_002467	−1.20	0.0351	transcription	apoptosis/G_1 to S cell cycle
CCNA2	NM_001237	−1.18	0.0112	cell cycle	cell cycle
CCNB2	NM_004701	−1.18	0.0152	cell cycle	cell cycle
PLK1	NM_005030	−1.20	0.0097	protein amino acid phosphorylation	cell cycle
CDC20	NM_001255	−1.19	0.0230	ubiquitin-dependent protein catabolic process	cell cycle
DBF4	NM_006716	−1.19	0.0337	G_1/S transition of mitotic cell cycle	cell cycle/DNA replication
CDKN2A	NM_000077	1.10	0.0144	cell cycle checkpoint	G_1 to S cell cycle
RB1	NM_000321	1.16	0.0229	cell cycle checkpoint G_1	G_1 to S cell cycle
TNXB	NM_019105	−1.19	0.0123	transcription	G_1 to S cell cycle
TNXA	NM_019105	−1.17	0.0039	transcription	G_1 to S cell cycle
INHBA	NM_002192	−1.22	0.0491	G_1/S transition of mitotic cell cycle	TGF-β signaling
ENG	NM_000118	−1.22	0.0083	transport	TGF-β signaling
MPO	NM_000250	−1.12	0.0132	antiapoptosis	
C17orf88	XR_017759	−1.21	0.0151	apoptosis	
DAP	NM_004394	−1.10	0.0234	apoptosis	
GAS2	NM_005256	−1.11	0.0131	apoptosis	
TNFRSF14	NM_003820	−1.11	0.0243	apoptosis	
MOAP1	NM_022151	1.12	0.0328	apoptosis	
CETN2	NM_004344	−1.17	0.0192	cell cycle	
NCAPG	NM_022346	−1.16	0.0182	cell cycle	
RBBP4	NM_005610	−1.13	0.0004	DNA replication	
RAD17	NM_002873	1.11	0.0205	DNA replication checkpoint	
GSPT1	NM_001130006	−1.21	0.0208	G_1/S transition of mitotic cell cycle	
RCC1	NM_001048194	−1.25	0.0228	G_1/S transition of mitotic cell cycle	
MPHOSPH6	NM_005792	−1.11	0.0104	M phase of mitotic cell cycle	
NUSAP1	NM_001129897	−1.25	0.0140	mitotic sister chromatid segretation	
BCL71	NM_001024808	−1.20	0.0348	negative regulation of transcription	
CDKN3	NM_001130851	−1.23	0.0077	regulation of cyclin-dependent protein kinase activity	
CKS2	NM_001827	−1.14	0.0134	regulation of cyclin-dependent protein kinase activity	
RBL2 (p130)	NM_005611	1.19	0.0053	transcription	

APP β-cleavage (18,39,41,43). In this respect, data have been reported indicating that APP β-cleavage is a cholesterol-dependent process occurring in the cholesterol-enriched lipid raft domains of the plasma membrane, through the action of the β-secretase (BACE1) enzyme (40) (see Fig. 3 for cholesterologenic enzymes). Our data indicated the inactivation of BACE1 gene along with the upregulation of the MUNC18C gene, which stabilizes APP on the plasma membrane, blocking the endogenous amyloidogenic pathway (25) (see Fig. 7 for a schematic view of all these molecular processes).

Thus, the increased fluidity of cell membranes determined by lower cholesterol levels, rather than the direct effect on the intracellular APP processing, might constitute the basis for the detrimental effects mediated by micromolar concentrations of S100B protein in this cellular model. We could assume that cells exposed to S100B are more vulnerable to toxic insults coming from the extracellular environment due to an imbalance of lipid homeostasis. More in general, S100B-induced low intracellular cholesterol levels could reasonably affect the integrity of intracellular membranes interfering with a number of cell functions including biosynthetic pathways and intracellular trafficking.

A quite unexpected effect induced by micromolar S100B in our model was a significant inhibition of cell proliferation: the reduced cell viability induced by S100B in the present experimental system is reasonably mediated, at least in part, by the transcriptional modulation of genes involved in cell cycle regulation and apoptosis. In particular, we observed the upregulation of the tumor suppressor retinoblastoma (RB1) gene and of the RB-linked genes p130 (RBL2) and p107 (RBL1; $p = 0.017$ and FC = 1.05, see complete gene list on GEO; http://www.ncbi.nlm.nih.gov/geo/, accession number GSE15218). The overexpression of these proteins can induce growth arrest in the G_1 phase (16). Furthermore, we observed the modulation of a number of nuclear molecules acting upstream of RB1, including the cyclin-dependent ki-

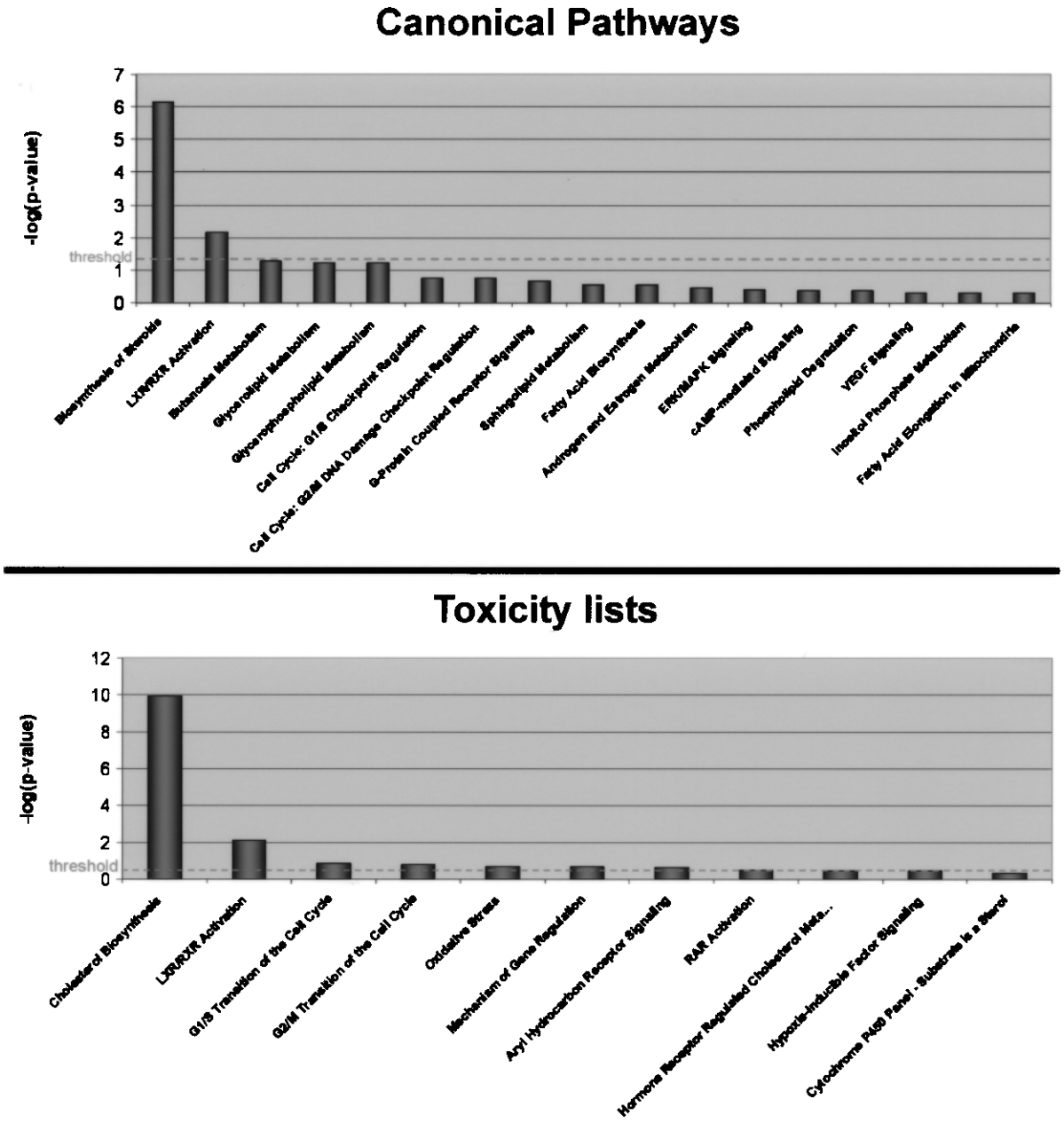

Figure 4. IPA analysis results. Top: The canonical pathways that are involved in this analysis are displayed along the *x*-axis; the *y*-axis displays the significance (–log *p*-value). The threshold line is set as default at $p = 0.05$. Bottom: Putative toxic molecules are grouped in lists displayed along the *x*-axis; the *y*-axis displays the significance (–log *p*-value). The threshold line is set as default at $p = 0.05$.

nase-D (CDK) inhibitor p16, which is upregulated. It has been reported that both reduced p16 activity and cyclin D1 overexpression produce persistent RB1 hyperphosphorylation, resulting in cell cycle arrest (21). Thus, p16 activity has a crucial role in blocking cells in a "nonproliferative" state (35). Our results also showed the downregulation of the oncogene MYC, coding for a multifunctional nuclear phosphoprotein that affects cyclin D1 and CDK4 activity. Other authors demonstrated that MYC downregulation in astrocytoma cells led to G_1 accumulation and inhibition of cell proliferation with S phase delay (2).

Previous reports indicated that S100B binds to the tumor suppressor p53 gene influencing its oligomerization state and its subcellular localization and function (19). In this regard, we have observed the transcriptional modulation of selected p53-interacting molecules: PERP was slightly upregulated, and

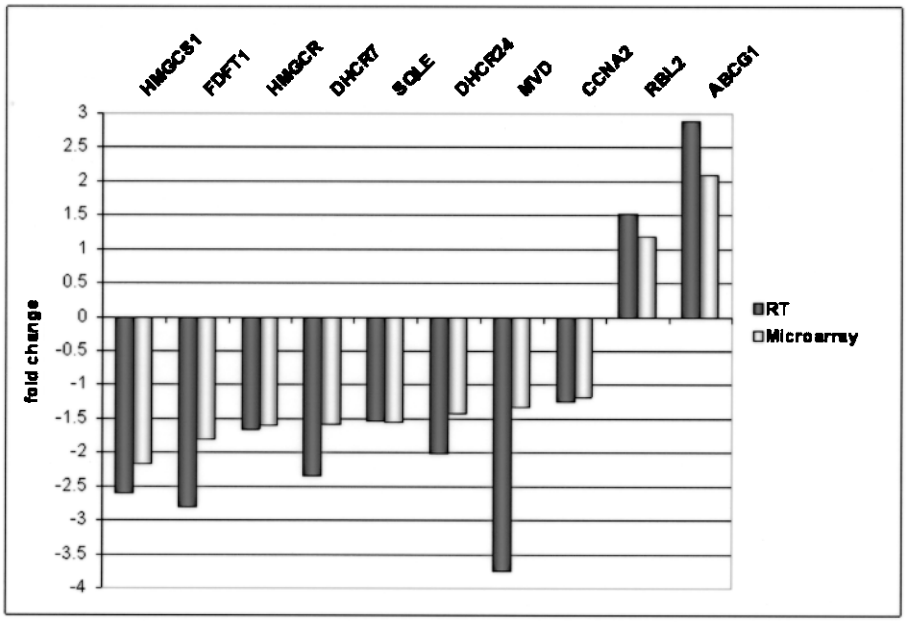

Gene	RT	Microarray
HMGCS1	-2.61	-2.16
FDFT1	-2.81	-1.80
HMGCR	-1.65	-1.60
DHCR7	-2.36	-1.59
SQLE	-1.54	-1.55
DHCR24	-2.02	-1.41
MVD	-3.75	-1.34
CCNA2	-1.25	-1.18
RBL2	1.53	1.19
ABCG1	2.88	2.08

Figure 5. Real-time PCR validation. Results of real-time PCR on selected genes. RT: fold change obtained in real time; Microarray: fold change obtained by means of microarray analysis.

CKS2 and CDC20 were both downregulated. Based on their reported functions, the final effect of the transcriptional modulation of p53 target genes should lead to G_2/M transition block (5,6,31).

On the whole, the direct effects of micromolar concentrations of S100B on cell viability of LAN-5 seemed to occur by blocking cell proliferation at the main cell cycle checkpoints, although this effect could be likely brought back at least in part to the higher mitogenic activity of LAN-5 cells. Thus, in light of the cell growth kinetics differences between mature neurons and neuroblasts, the present finding might not perfectly suit for understanding the mechanisms of S100B detrimental effects on neurons. Nonetheless, the cell growth potential of neuroblasts replacing dead neurons could be considered as an additional key for the interpretation of these data. This would possibly suggest that the effect of micromolar

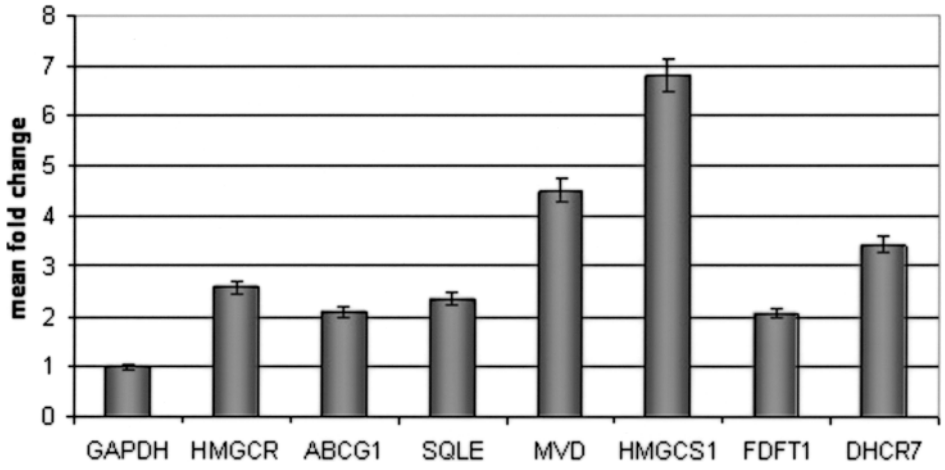

Figure 6. Gene expression in 50 nM S100B-treated cells. Results of real-time PCR for selected genes involved in the cholesterologenic pathway. Fold change values are expressed as mean ± SD of replicated experiments.

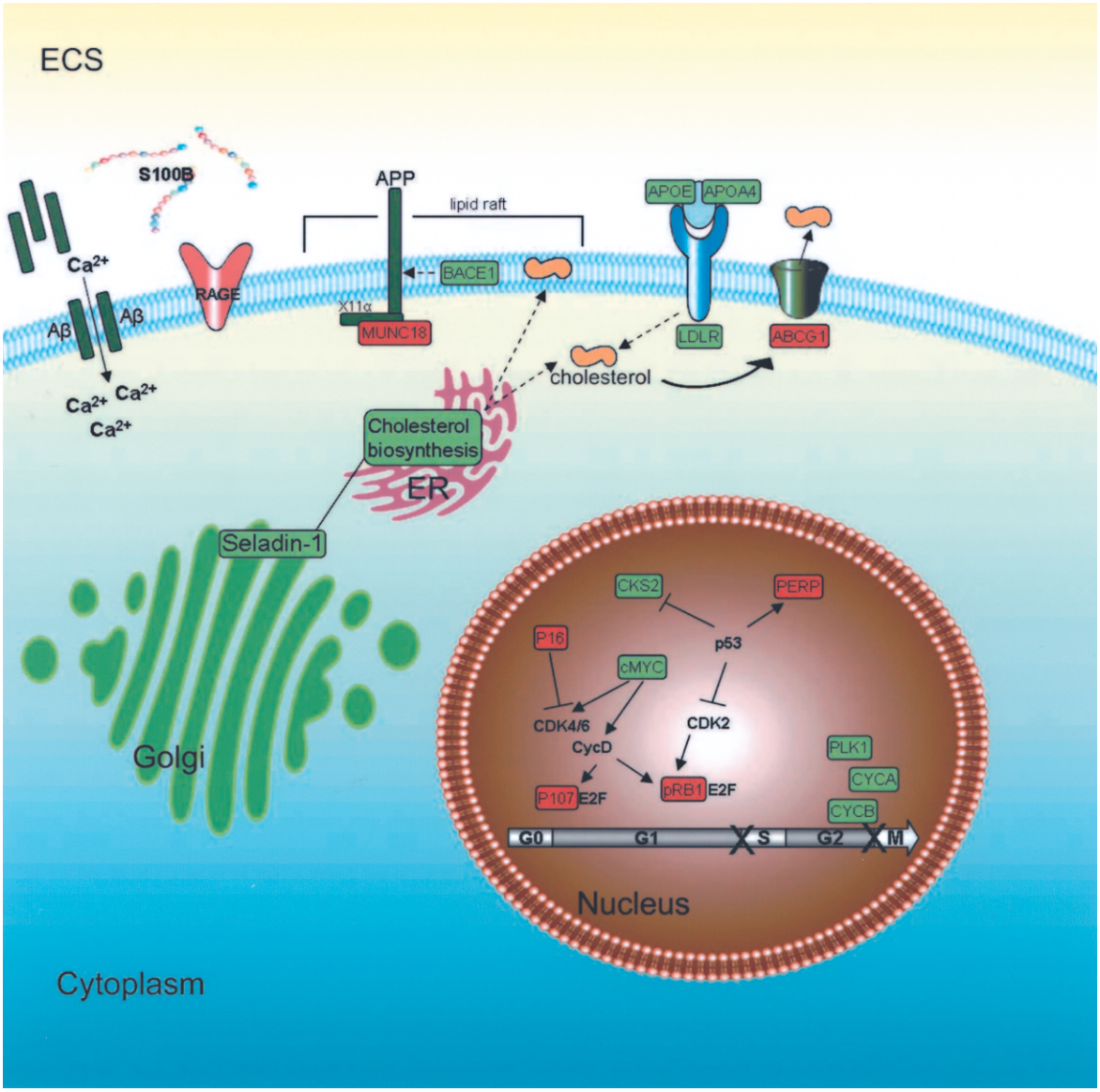

Figure 7. Interactions between membrane–lipid metabolism, APP processing and β-secretase (BACE) activity, cholesterol uptake/efflux and cell cycle regulation. Upregulated genes appear in red boxes, downregulated genes in green boxes. Biosynthesis of endogenous cholesterol is inhibited (broken arrows) as genes coding for critical enzymes in this pathway, including Seladin-1, are downregulated. Aβ peptide channel-forming activity, allowed by cholesterol depletion in this model, could increase calcium influx (left upper corner of the image). Exogenous cholesterol uptake (APOA4, APOE, LDLR) is downregulated while ABCG1, responsible of cholesterol efflux from cells, is upregulated. As a result of gene regulation observed in this experimental model, the amyloidogenic cleavage of APP seemed to be inhibited. Inside the nucleus, the modulation of genes involved in cell cycle regulation and apoptosis led to both G_1/S and G_2/M arrest, resulting in the inhibition of proliferation (see text for details). ECS, extracellular space; ER, endoplasmic reticulum.

S100B could be also the result of the interference exerted on the regenerative process, rather than a direct effect on differentiated cells.

In conclusion, considering the transcriptional effects observed in lipid homeostasis, the present study proposed new clues toward the definition of an active role of S100B in neurodegenerative processes. Reasonably, a different pattern of gene expression profiling should be expected after administration of nanomolar S100B, because the protein is not known to display any role in neurodegenerative processes at this concentration. Finally, well-established evidences indicating the reliability of S100B as a marker of active brain injury should also be considered in light of these findings, which could help to clarify the molecular cascade of events triggered by S100B in cells.

ACKNOWLEDGMENT

This work was supported in part by PRIN-COFIN 2008 (L.F.).

REFERENCES

1. Allore, R.; O'Hanlon, D.; Price, R.; Neilson, K.; Willard, H. F.; Cox, D. R.; Marks, A.; Dunn, R. J. Gene encoding the beta subunit of S100 protein is on chromosome 21: Implications for Down syndrome. Science 23:1311–1313; 1988.
2. Amendola, D.; De Salvo, M.; Marchese, R.; Verga Falzacappa, C.; Stigliano, A.; Carico, E.; Brunetti, E.; Moscarini, M.; Bucci, B. Myc down-regulation affects cyclin D1/cdk4 activity and induces apoptosis via Smac/Diablo pathway in an astrocytoma cell line. Cell Prolif. 42:94–109; 2009.
3. Arispe, N.; Doh, M. Plasma membrane cholesterol controls the cytotoxicity of Alzheimer's disease AbetaP (1–40) and (1–42) peptides. FASEB J. 16:1526–1536; 2002.
4. Ashburner, M.; Ball, C. A.; Blake, J. A.; Botstein, D.; Butler, H.; Cherry, J. M.; Davis, A. P.; Dolinski, K.; Dwight, S. S.; Eppig, J. T.; Harris, M. A.; Hill, D. P.; Issel-Tarver, L.; Kasarskis, A.; Lewis, S.; Matese, J. C.; Richardson, J. E.; Ringwald, M.; Rubin, G. M.; Sherlock, G. Gene ontology: Tool for the unification of biology. The Gene Ontology Consortium. Nat. Genet. 25:25–29; 2000.
5. Attardi, L. D.; Reczek, E. E.; Cosmas, C.; Demicco, E. G.; McCurrach, M. E.; Lowe, S. W.; Jacks, T. PERP, an apoptosis-associated target of p53, is a novel member of the PMP-22/gas3 family. Genes Dev. 14: 704–718; 2000.
6. Banerjee, T.; Nath, S.; Roychoudhury, S. DNA damage induced p53 downregulates Cdc20 by direct binding to its promoter causing chromatin remodeling. Nucleic Acids Res. 37:2688–2698; 2009.
7. Bolstad, B. M.; Irizarry, R. A.; Astrand, M.; Speed, T. P. A comparison of normalization methods for high density oligonucleotidearray data based on variance and bias. Bioinformatics 19:185–193; 2003.
8. Brazma, A.; Hingamp, P.; Quackenbush, J.; Sherlock, G.; Spellman, P.; Stoeckert, C.; Aach, J.; Ansorge, W.; Ball, C. A.; Causton, H. C.; Gaasterland, T.; Glenisson, P.; Holstege, F. C.; Kim, I. F.; Markowitz, V.; Matese, J. C.; Parkinson, H.; Robinson, A.; Sarkans, U.; Schulze-Kremer, S.; Stewart, J.; Taylor, R.; Vilo, J.; Vingron, M. Minimum information about a microarray experiment (MIAME)-toward standards for microarray data. Nat. Genet. 29:365–371; 2001.
9. Businaro, R.; Leone, S.; Fabrizi, C.; Sorci, G.; Donato, R.; Lauro, G. M.; Fumagalli, L. S100B protects LAN-5 neuroblastoma cells against Abeta amyloid-induced neurotoxicity via RAGE engagement at low doses but increases Abeta amyloid neurotoxicity at high doses. J. Neurosci. Res. 83:897–906; 2006.
10. Carter, C. J. Convergence of genes implicated in Alzheimer's disease on the cerebral cholesterol shuttle: APP, cholesterol, lipoproteins, and atherosclerosis. Neurochem. Int. 50:12–38; 2007.
11. Cecchi, C.; Rosati, F.; Pensalfini, A.; Formigli, L.; Nosi, D.; Liguri, G.; Dichiara, F.; Morello, M.; Danza, G.; Pieraccini, G.; Peri, A.; Serio, M.; Stefani, M. Seladin-1/DHCR24 protects neuroblastoma cells against Abeta toxicity by increasing membrane cholesterol content. J. Cell. Mol. Med. 12:1990–2002; 2008.
12. Chen, L.; Na, R.; Gu, M.; Richardson, A.; Ran, Q. Lipid peroxidation up-regulates BACE1 expression in vivo: A possible early event of amyloidogenesis in Alzheimer's disease. J. Neurochem. 107:197–207; 2008.
13. Craft, J. M.; Watterson, D. M.; Marks, A.; Van Eldik, L. J. Enhanced susceptibility of S-100B transgenic mice to neuroinflammation and neuronal dysfunction induced by intracerebroventricular infusion of human beta-amyloid. Glia 51(3):209–216; 2005.
14. Donato, R. Calcium-independent, pH-regulated effects of S-100 proteins on assembly-disassembly of brain microtubule protein in vitro. J. Biol. Chem. 263:106–110; 1988.
15. Donato, R.; Sorci, G.; Riuzzi, F.; Arcuri, C.; Bianchi, R.; Brozzi, F.; Tubaro, C.; Giambanco, I. S100B's double life: Intracellular regulator and extracellular signal. Biochim. Biophys. Acta 1793:1008–1022; 2009.
16. Dyson, N. The regulation of E2F by pRB-family proteins. Genes Dev. 12:2245–2262; 1998.
17. Esposito, G.; Scuderi, C.; Lu, J.; Savani, C.; De Filippis, D.; Iuvone, T.; Steardo, Jr., L.; Sheen, V.; Steardo, L. S100B induces tau protein hyperphosphorylation via Dickopff-1 up-regulation and disrupts the Wnt pathway in human neural stem cells. J. Cell. Mol. Med. 12(3):914–927; 2008.
18. Fassbender, K.; Simons, M.; Bergmann, C.; Stroick, M.; Lutjohann, D.; Keller, P.; Runz, H.; Kuhl, S.; Bertsch, T.; von Bergmann, K.; Hennerici, M.; Beyreuther, K.; Hartmann, T. Simvastatin strongly reduces levels of Alzheimer's disease beta-amyloid peptides Abeta 42 and Abeta 40 in vitro and in vivo. Proc. Natl. Acad. Sci. USA 98:5856–5861; 2001.
19. Fernandez-Fernandez, M. R.; Veprintsev, D. B.; Fersht, A. R. Proteins of the S100 family regulate the oligomerization of p53 tumor suppressor. Proc. Natl. Acad. Sci. USA 102:4735–4740; 2005.
20. Gazzolo, D.; Bruschettini, M.; Corvino, V.; Lituania, M.; Sarli, R.; Bruschettini, P.; Michetti, F. Amniotic fluid levels of S100B protein in normal and trisomy-21 foetuses. Clin. Chim. Acta 330:131–133; 1988.
21. Giacinti, C.; Giordano, A. RB and cell cycle progression. Oncogene 25:5220–5227; 2006.
22. Gonçalves, C. A.; Leite, M. C.; Nardin, P. Biological and methodological features of the measurement of S100B, a putative marker of brain injury. Clin. Biochem. 41:755–763; 2008.
23. Greeve, I.; Hermans-Borgmeyer, I.; Brellinger, C.; Kasper, D.; Gomez-Isla, T.; Behl, C.; Levkau, B.; Nitsch, R. M. The human DIMINUTO/DWARF1 homolog seladin-1 confers resistance to Alzheimer's disease-associated neurodegeneration and oxidative stress. J. Neurosci. 20:7345–7352; 2000.
24. Hansen, M. B.; Nielsen, S. E.; Berg, K. Re-examination and further development of a precise and rapid dye method for measuring cell growth/cell kill. J. Immunol. Methods 119:203–210; 1989.

25. Ho, C. S.; Marinescu, V.; Steinhilb, M. L.; Gaut, J. R.; Turner, R. S.; Stuenkel, E. L. Synergistic effects of Munc18a and X11 proteins on amyloid precursor protein metabolism. J. Biol. Chem. 277:27021–27028; 2002.
26. Huttunen, H. J.; Kuja-Panula, J.; Sorci, G.; Agneletti, A. L.; Donato, R.; Rauvala, H. Coregulation of neurite outgrowth and cell survival by amphoterin and S100 proteins through receptor for advanced glycation end products (RAGE) activation. J. Biol. Chem. 275: 40096–40105; 2000.
27. Iivonen, S.; Hiltunen, M.; Alafuzoff, I.; Mannermaa, A.; Kerokoski, P.; Puoliväli, J.; Salminen, A.; Helisalmi, S.; Soininen, H. Seladin-1 transcription is linked to neuronal degeneration in Alzheimer's disease. Neuroscience 113(2):301–310; 2002.
28. Irizarry, R. A.; Hobbs, B.; Collin, F.; Beazer-Barclay, Y. D.; Antonellis, K. J.; Scherf, U.; Speed, T. P. Exploration, normalization, and summaries of high density oligonucleotide array probe level data. Biostatistics 4:249–264; 2003.
29. Lattanzi, W.; Bernardini, C.; Gangitano, C.; Michetti, F. Hypoxia-like transcriptional activation in TMT-induced degeneration: Microarray expression analysis on PC12 cells. J. Neurochem. 100:1688–1702; 2007.
30. Livak, K. J.; Schmittgen, T. D. Analysis of relative gene expression data using real-time quantitative PCR and the 2(-Delta Delta C(T)) method. Methods 25:2–8; 2001.
31. Martinsson-Ahlzén, H. S.; Liberal, V.; Grünenfelder, B.; Chaves, S. R.; Spruck, C. H.; Reed, S. I. Cyclin-dependent kinase-associated proteins Cks1 and Cks2 are essential during early embryogenesis and for cell cycle progression in somatic cells. Mol. Cell. Biol. 28: 5698–5709; 2008.
32. Michetti, F.; Gazzolo, D. S100B protein in biological fluids: A tool for perinatal medicine. Clin. Chem. 48: 2097–2104; 1980.
33. Michetti, F.; Massaro, A.; Russo, G.; Rigon, G. The S100 antigen in cerebrospinal fluid as a possible index of cell injury in the nervous system. J. Neurol. Sci. 44: 259–263; 1980.
34. Moore, B. W. A soluble protein characteristic of the nervous system. Biochem. Biophys. Res. Commun. 19: 739–744; 1965.
35. Pajalunga, D.; Mazzola, A.; Salzano, A. M.; Biferi, M. G.; De Luca, G.; Crescenzi, M. Critical requirement for cell cycle inhibitors in sustaining nonproliferative states. J. Cell Biol. 176:807–818; 2007.
36. Peña, L. A.; Brecher, C. W.; Marshak, D. R. beta-Amyloid regulates gene expression of glial trophic substance S100 beta in C6 glioma and primary astrocyte cultures. Brain Res. Mol. Brain Res. 34:118–126; 1995.
37. Pensalfini, A.; Zampagni, M.; Liguri, G.; Becatti, M.; Evangelisti, E.; Fiorillo, C.; Bagnoli, S.; Cellini, E.; Nacmias, B.; Sorbi, S.; Cecchi, C. Membrane cholesterol enrichment prevents Aβ-induced oxidative stress in Alzheimer's fibroblasts. Neurobiol. Aging; in press.
38. Peri, A.; Serio, M. Neuroprotective effects of the Alzheimer's disease-related gene seladin-1. J. Mol. Endocrinol. 41:251–261; 2008.
39. Refolo, L. M.; Malester, B.; LaFrancois, J.; Bryant-Thomas, T.; Wang, R.; Tint, G. S.; Sambamurti, K.; Duff, K.; Pappolla, M. A. Hypercholesterolemia accelerates the Alzheimer's amyloid pathology in a transgenic mouse model. Neurobiol. Dis. 7:321–331; 2000.
40. Reid, P. C.; Urano, Y.; Kodama, T.; Hamakubo, T. Alzheimer's disease: Cholesterol, membrane rafts, isoprenoids and statins. J. Cell. Mol. Med. 11:383–392; 2007.
41. Sakurai, T.; Kaneko, K.; Okuno, M.; Wada, K.; Kashiyama, T.; Shimizu, H.; Akagi, T.; Hashikawa, T.; Nukina, N. Membrane microdomain switching: A regulatory mechanism of amyloid precursor protein processing. J. Cell Biol. 183:339–352; 2008.
42. Sen, J.; Belli, A. S100B in neuropathologic states: The CRP of the brain? J. Neurosci. Res. 85:1373–1380; 2007.
43. Simons, M.; Keller, P.; De Strooper, B.; Beyreuther, K.; Dotti, C. G.; Simons, K. Cholesterol depletion inhibits the generation of beta-amyloid in hippocampal neurons. Proc. Natl. Acad. Sci. USA 95:6460–6464; 1998.
44. Sorci, G.; Riuzzi, F.; Agneletti, A. L.; Marchetti, C.; Donato, R. S100B causes apoptosisin a myoblast cell line in a RAGE-independent manner. J. Cell Physiol. 199(2):274–283; 2004.
45. Tsoporis, J. N.; Izhar, S.; Leong-Poi, H.; Desjardins, J. F.; Huttunen, H. J.; Parker, T. G. S100B interaction with the receptor for advanced glycation end products (RAGE): A novel receptor-mediated mechanism for myocyte apoptosis postinfarction. Circ. Res. 106(1): 93–101; 2010.
46. Van Eldik, L. J.; Wainwright, M. S. The Janus face of glial-derived S100B: Beneficial and detrimental functions in the brain. Restor. Neurol. Neurosci. 21:97–108; 2003.
47. Wainwright, M. S.; Craft, J. M.; Griffin, W. S.; Marks, A.; Pineda, J.; Padgett, K. R.; Van Eldik, L. J. Increased susceptibility of S100B transgenic mice to perinatal hypoxia-ischemia. Ann. Neurol. 56(1):61–67; 2004.
48. Wang, Y.; Rogers, P. M.; Stayrook, K. R.; Su, C.; Varga, G.; Shen, Q.; Nagpal, S.; Burris, T. P. The selective Alzheimer's disease indicator-1 gene (Seladin-1/DHCR24) is a liver X receptor target gene. Mol. Pharmacol. 74:1716–1721; 2008.
49. Whitney, K. D.; Watson, M. A.; Collins, J. L.; Benson, W. G.; Stone, T. M.; Numerick, M. J.; Tippin, T. K.; Wilson, J. G.; Winegar, D. A.; Kliewer, S. A. Regulation of cholesterol homeostasis by the liver X receptors in the central nervous system. Mol. Endocrinol. 16: 1378–1385; 2002.
50. Winningham-Major, F.; Staecker, J. L.; Barger, S. W.; Coats, S.; Van Eldik, L. J. Neurite extension and neuronal survival activities of recombinant S100 beta proteins that differ in the content and position of cysteine residues. J. Cell Biol. 109:3063–3071; 1989.
51. Wu, Z.; Irizarry, R. A. A statistical framework for the

analysis of microarray probe-level data. Johns Hopkins University, Dept. of Biostatistics Working Papers. Working Paper 73 [http://www.bepress.com/jhubiostat/paper73]; 2005.
52. Zelcer, N.; Khanlou, N.; Clare, R.; Jiang, Q.; Reed-Geaghan, E. G.; Landreth, G. E.; Vinters, H. V.; Tontonoz, P. Attenuation of neuroinflammation and Alzheimer's disease pathology by liver x receptors. Proc. Natl. Acad. Sci. USA 104:10601–10606; 2007.